

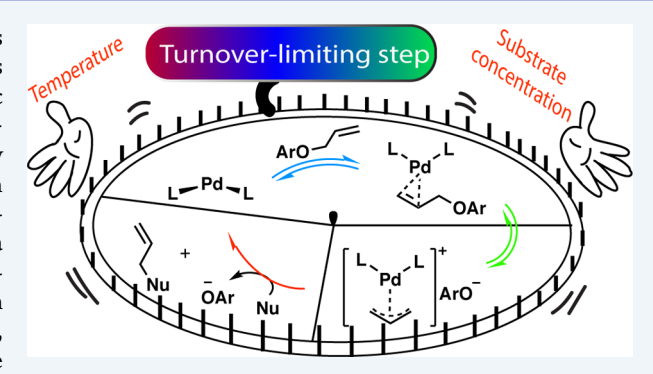
Kinetics and Inverse Temperature Dependence of a Tsuji-Trost Reaction in Aqueous Buffer

Ivanna Pohorilets,[†] Matthew P. Tracey,[†] Michael J. LeClaire, Emily M. Moore, Gang Lu, Peng Liu,* and Kazunori Koide*

Department of Chemistry, University of Pittsburgh 219 Parkman Avenue, Pittsburgh, Pennsylvania 15260, United States

Supporting Information

ABSTRACT: The palladium-catalyzed Tsuji—Trost reaction has been extensively studied under synthetically relevant conditions (millimolar concentrations of substrates and catalyst, aprotic solvents, no additives). Despite the increasing use of the Tsuji—Trost reaction in other areas (e.g., chemical biology), the paucity of kinetic studies at micromolar concentrations of substrates in water has impeded progress. Herein, we show that a fluorescence-based high-throughput method provided massive Eyring plot data and revealed three kinetic regimes. The associated turnoverlimiting steps (TLSs) were assigned as the oxidative addition (regime 1; $\Delta H^{\ddagger} > 0$), nucleophilic attack (regime 2; $\Delta H^{\ddagger} \approx 0$), and association (regime 3; $\Delta H^{\ddagger} < 0$, inverse temperature dependence). A kinetic profile under particular conditions



depended on the substrate concentration and reaction temperature. Density functional theory calculations supported these findings. This work indicates that a TLS under dilute conditions may be different from that under synthetically relevant conditions and may provide a path toward the development of faster and more reproducible Tsuji—Trost reactions for synthetic, analytical, and biological applications.

KEYWORDS: palladium, allyl, kinetics, DFT, Tsuji-Trost, phosphate

■ INTRODUCTION

The palladium-catalyzed Tsuji-Trost reaction is useful not only in synthetic organic chemistry 1-3 but also in the development of chemosensors, 4-9 signal amplification, 10 and bioorthogonal chemistry. 11-16 The kinetics of the Tsuji–Trost reaction have been extensively studied at millimolar concentrations in aprotic solvents, where palladium species may aggregate and make it difficult to study the system. 17 Nonetheless, at these concentrations the turnover-limiting step (TLS) can be either oxidative addition or nucleophilic attack (Scheme 1a).18 For example, with linear substrates, the $(\pi$ -allyl)palladium complex is the resting state of the catalytic cycle, with nucleophilic attack being rate-determining. 19-21 The nucleophile can attack the carbon or the metal center (also known as outer sphere and inner sphere, respectively; Scheme 1b). Soft nucleophiles attack the carbon center directly through the outer sphere.³ In contrast, hard nucleophiles attack the metal center via the inner sphere, and the carbon-carbon bond formation occurs after reductive elimination. With cyclic substrates, the TLS may be the oxidative addition of palladium(0) to an allylic C-O bond.²²

In addition to the kinetic studies, mechanistic investigations have elucidated the structures of actual catalysts. For example, $(\pi$ -allyl)palladium with two phosphine ligands is generally considered a key intermediate, ²¹ but the complex with a single

phosphine may be more reactive. ^{23,24} Palladium dimers have also been shown to be active catalysts in some instances. ²⁵

In recent years, the Tsuji—Trost reaction in alcohols and water has garnered interest in synthetic, analytical, and biological chemistry. Many groups, including ours, reported fluorometric palladium detection methods for pharmaceutical applications on the basis of the Tsuji—Trost reaction. 4,26 We discovered that tris(2-furyl)phosphine (TFP) was one of the best ligands to accelerate the palladium-catalyzed allylic C—O bond cleavage. 27–30 Consequently, one of the methods from our laboratory using TFP has been implemented in the pharmaceutical industry for palladium quantification. 29,31 However, generally when palladium-catalyzed Tsuji—Trost reactions are studied for the fluorometric quantification of palladium, reaction temperatures and concentrations of components appear to be arbitrarily chosen, with no obvious justification.

In bioorthogonal chemistry, palladium-catalyzed removal of an allyl moiety from a key functional group has emerged as a method to uncage bioactive compounds inside and outside of live cells. 32–36 However, such a reaction with phosphine-less palladium species was deemed too slow to be viable for

Received: July 16, 2019
Revised: November 2, 2019
Published: November 8, 2019



Scheme 1. (a) General Catalytic Cycle of a Tsuji-Trost Reaction and (b) Two Modes of Nucleophilic Attack between Hard and Soft Nucleophiles

 a R = COCH₃, COPh, Ph, etc. R' = aryl or alkyl group.

biological studies.^{34,35} It should be noted that, during our current study, the Weissleder group showed that TFP-bound palladium could catalyze the deallylation in mice.²⁷ Their work indicates that the combination of TFP and palladium may prove to be a powerful bioorthogonal tool. Despite their promising results, the palladium-catalyzed deallylation is considered too slow to be useful in biology.³⁷

To develop robust and faster palladium-catalyzed Tsuji-Trost reactions, it is paramount to identify their TLSs under relevant conditions. This is especially critical for analytical and biological applications, because catalysts and substrates are at unorthodox, nano- to micromolar concentrations. Moreover, the effects of temperature, DMSO, and phosphate ions are poorly understood. Herein, we report that the TLS changes in Tsuji-Trost reactions and that the activation of enthalpy was negative in one of the three kinetic regimes. In these regimes, the reaction rates are differentially influenced by the concentrations of DMSO and phosphate ions. The inversion temperatures depend on the substrate concentration. These findings may allow others to rationally design the reaction conditions of Tsuji-Trost reactions and improve reproducibility. This work may contradict a perception that the reaction is well-understood.³

RESULTS AND DISCUSSION

We previously reported the palladium-catalyzed deallylation of the fluorogenic chemodosimeter allyl Pittsburgh Green ether (APE; Scheme 2) in 5% DMSO/pH 7 buffer. Bittsburgh Green represents typical leaving groups in Tsuji—Trost reactions because the pK_a value of the phenolic hydroxyl group is 4.27, Preflecting the acidity of carboxylic acids or electron-deficient phenols. As the Semagina group demonstrated, the use of APE for mechanistic studies can provide new insights because the reaction can be both continuously and accurately monitored by fluorescence at low micromolar concentrations.

The reaction proceeded more quickly when we replaced Ph₃P with TFP⁴¹ and when we increased the phosphate concentration from 0.05 to 1.23 M.⁴² As shown below, the use of NaBH₄ did not have an effect on the conclusion of this paper but facilitated kinetic studies; it eliminated the deactivation of palladium(0) by air oxidation when high-throughput experiments were carried out under an air

Scheme 2. Deallylation of Nonfluorescent Allyl Pittsburgh Green Ether to Fluorescent Pittsburgh Green

atmosphere.²⁹ If palladium nanoparticles are formed under the reaction conditions, it would complicate the interpretation of data. However, because the solvents in this study are DMSO and water and palladium concentrations are in the 10 nM to 4 μ M range, palladium species are most likely monomeric.⁴³

Figure 1a shows the consumption of 50 or 25 μ M APE over time. Fitting the consumption of APE to a one-phase decay model revealed that the reaction rapidly slowed as the substrate concentration approached 4 μ M (Table 1). When the reaction started with 5 μ M APE, the reaction progressed at a rate similar to that when the above reaction slowed after the substrate concentration reached 4 μ M, excluding product inhibition and indicating that the TLS may change at this concentration (Figure 1b and Table 1). If the TLS remains the same during the course of the reaction, a single kinetic profile should be observed from 50 to 0 μ M. As this was not the case, we turned to Eyring plots to quantify energetic contributions in the reaction.

The preparation of an Eyring plot involves plotting the natural log of the reaction rate constant against the inverse temperature to afford a line where the slope is $-\Delta H^{\ddagger}/R$ and

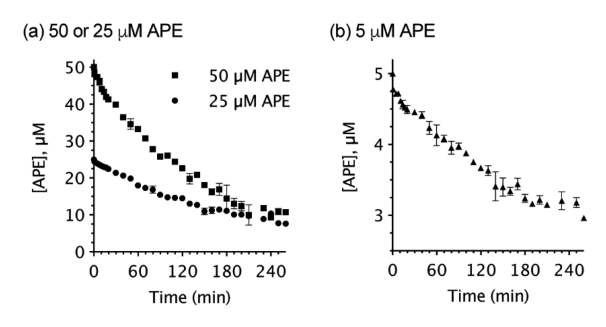


Figure 1. Consumption of APE as a function of time. Conditions: (a) 25 or 50 μ M APE, 1 μ M Pd(NO₃)₂, 80 μ M TFP, 10 mM NaBH₄, 10% v/v DMSO/1.23 M phosphate pH 7 buffer, 298 K; (b) 5 μ M APE, 1 μ M Pd(NO₃)₂, 80 μ M TFP, 10 mM NaBH₄, 10% v/v DMSO/1.23 M phosphate pH 7 buffer, 298 K. The data are available in Table S1 in the Supporting Information.

Table 1. Calculated Plateau of APE from Fitting to a One-Phase Decay as the Reaction Continues Indefinitely^a

initial APE concentration, μM	calculated plateau of APE (M) as reaction proceeds infinitely
5	$(8.0 \pm 4.0) \times 10^{-7}$
25	$(4.1 \pm 0.7) \times 10^{-6}$
50	$(4.1 \pm 1.3) \times 10^{-6}$

^aData over time are also shown in Figure 1. Conditions: 5, 25, or 50 μ M APE, 1 μ M Pd(NO₃)₂, 80 μ M TFP, 10 mM NaBH₄, 10% DMSO v/v 1.23 M phosphate pH 7 buffer.

the y intercept is $\ln(k_b/T) + \Delta S^{\ddagger}/R$ (Figure S1). ΔH^{\ddagger} values are intrinsically independent of the concentrations of reactants, while ΔS^{\ddagger} values are often dependent. Since it was not possible to measure the concentrations of reactive species involved in the TLS, this article will not discuss experimental ΔS^{\ddagger} values extensively. We measured the fluorescence stemming from the reaction product (Pittsburgh Green, Scheme 2) after 30 min, at which point a vast majority of the substrate remained intact. This choice allowed for high-throughput and accurate data collection under analytically and biologically relevant, highly diluted conditions in a 96-well format.

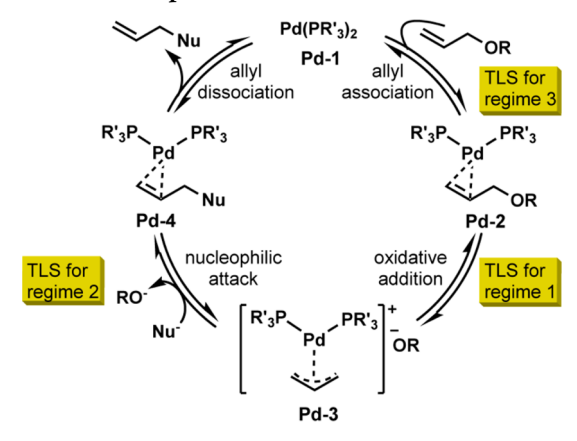
Initial Investigation with Previously Optimized Conditions: Effect of Substrate Concentration. We first wished to establish a benchmark Eyring plot under previously optimized conditions ⁴² at 293–358 K. With 12.5 μ M APE, we uncovered three regimes (Figure 2a). Regime 1, regime 2, and regime 3 showed $\Delta H^{\ddagger} > 0$, $\Delta H^{\ddagger} \approx 0$, and $\Delta H^{\ddagger} < 0$, respectively. The concave-down shape may indicate two changes in TLS ^{444–47} (for quantitative data, see Table S3 in

the Supporting Information). These benchmark values for ΔH^{\ddagger} provided a standard against which we could evaluate effects on the TLS by changing conditions, using the generally accepted mechanism (Scheme 1a).

We then used APE at 25 and 50 μ M concentrations; the APE concentrations had little effect on ΔH^{\ddagger} in regime 1 (42–55 kJ/mol; Figure 2a) but had a notable effect on the inversion temperature $(T_{\rm inv})$. Specifically, when the APE concentration was lower, the $T_{\rm inv}$ value was lower (Figure 2b). This observation can account for the change observed in Figure 1; as the reaction proceeds, the kinetic profile at a specific reaction temperature shifts from regime 1 to regime 2 and finally to regime 3 (Figure 2b, "specific temperature"). The existence of regime 2 was uncertain at this point, because this regime might be the transition between regime 1 and regime 3. However, further studies shown below support the existence of regime 2 as an independent regime.

For regime 1, we propose that the TLS is oxidative addition (i.e., Pd-2 to Pd-3, Scheme 3) because this step converts the

Scheme 3. General Catalytic Cycle of a Tsuji-Trost Reaction with Proposed TLSs



stronger C–O bond to the weaker Pd–O and Pd–C bonds. For regime 2, the TLS is entropically controlled; this may be attributed to the nucleophilic attack toward Pd-3, as will be discussed later. Regime 3 is inversely temperature dependent $(\Delta H^{\ddagger} < 0)$, which is scarce in the literature and is not well understood. We propose that the TLS for regime 3 is the association of the TFP-ligated palladium species to the allyl group (i.e., Pd-1 to Pd-2) as the coordinatively unsaturated 14-electron species Pd-1 gains electrons to form the more stable 16-electron species Pd-2. As shown later, increasing

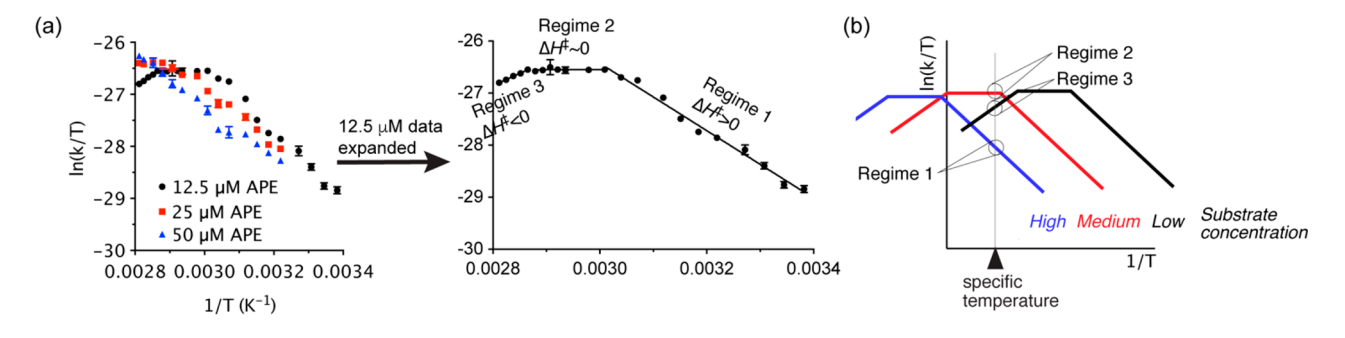


Figure 2. (a) Eyring plot under the previously developed reaction conditions with various APE concentrations: 9.4 nM Pd(NO₃)₂, 120 μ M TFP, 10 mM NaBH₄, 5% v/v DMSO, 1.23 M phosphate pH 7 buffer, 30 min. The raw data are available in Table S2 in the Supporting Information. (b) Changing regime with reaction progress at a single temperature.

palladium concentration eliminates this regime, supporting the association as the TLS of this regime.

Altogether, the identities of TLSs depend on both the temperatures and the substrate concentrations, and at elevated temperatures with very low substrate concentrations, ΔH^{\ddagger} has a negative value. To better understand the contributions of each reaction component on the kinetics, we began to systematically perturb the benchmark reaction conditions.

Effect of Phosphine Concentration. Numerous studies have shown that phosphine structures substantially affect palladium catalysis; $^{62-64}$ however, fewer have demonstrated correlations between phosphine concentration and reaction rate. 65,66 We studied the deallylation with 60, 120, and 180 μ M TFP; with 12.5 μ M APE (Figure 3a), the results did not differ

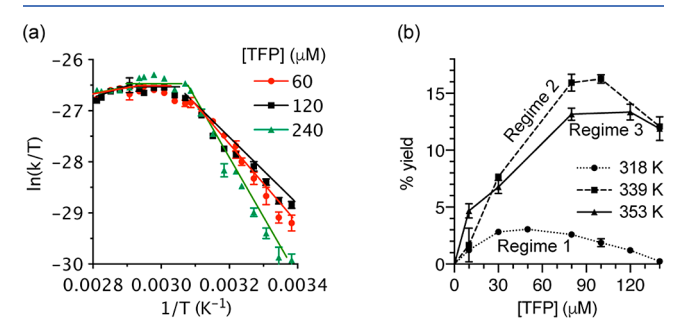


Figure 3. (a) Eyring plot with various TFP concentrations. Conditions: 9.4 nM Pd(NO₃)₂, 10 mM NaBH₄, 12.5 μ M APE, 5% v/v DMSO/1.23 M phosphate pH 7 buffer, 30 min. n=3. The raw data are available in Table S4 in the Supporting Information. (b) TFP-concentration dependence. Conditions: 0–140 μ M TFP, 9.4 nM Pd(NO₃)₂, 10 mM NaBH₄, 12.5 μ M APE, 5% v/v DMSO/1.23 M phosphate pH 7 buffer, 30 min. n=3. The raw data are available in Table S6 in the Supporting Information.

significantly at the three TFP concentrations (for quantitative data, see Table S5 in the Supporting Information). The correlation between the TFP concentration and deallylation rate showed an initial linear relationship at 318 K (regime 1), 339 K (regime 2), and 353 K (regime 3) (Figure 3b). At these three temperatures, the rate decreased with higher concentrations of TFP. This may be because the equilibrium between

less ligated and more highly ligated palladium species shift toward the latter at higher TFP concentrations. 65,67

Effect of Phosphate Ion Concentration. The Baran and Gaunt groups independently reported an unspecified but positive role of phosphate ions in palladium catalysis. ^{68,69} In more closely related systems, $(\pi$ -allyl)palladium—organic phosphate complexes were reactive intermediates, but the reactions were carried out in aprotic solvents (toluene, THF). ^{70,71} We wondered whether inorganic phosphates, originally intended to be used as the buffer salts, affect the deallylation kinetics in water. It should be noted that phosphate ions were not nucleophiles toward an electrophilic allyl species. ⁴² With 12.5 μ M substrate, we were unable to conclude whether and how phosphate ion concentrations influence the kinetic profile (Figure 4a).

Therefore, we resorted to a slightly different approach; the reaction was monitored at various phosphate concentrations at three temperatures corresponding to three regimes (Figure 4b). In this experiment, we did not use NaBH₄ because it would change the pH at low phosphate concentrations and because NaBH₄ was found to be unnecessary (see the section below). In regime 1 (318 K), the reaction rate was first order with respect to phosphate. In regimes 2 and 3 (339 and 353 K, respectively), the rates appeared to be nearly second order with respect to phosphate concentrations. Therefore, in regime 1 where the TLS may be the oxidative addition step, one molecule of a phosphate ion may be involved in the transition state. In regime 2 or regime 3 where the TLS may be nucleophilic attack or palladium—olefin association, two phosphate ions may be involved.

Crystal structures of palladium(II)—diphosphate complexes have been previously reported, ^{72,73} but palladium(0)—phosphate complexes have not been synthesized. A working hypothesis is depicted in Figure 4c; in the allyl association step, the palladium species may be bound to two phosphate ions, which are dissociated as the olefin binds the metal. The rate acceleration by phosphate ions may be due to the shift in equilibrium between phosphate-bound palladium as a precatalyst and DMSO-bound palladium as a resting state complex toward the precatalyst. In the oxidative addition step, either H₂PO₄⁻ or HPO₄²⁻ may form a hydrogen bond with the allylic oxygen atom to facilitate the C–O bond cleavage.

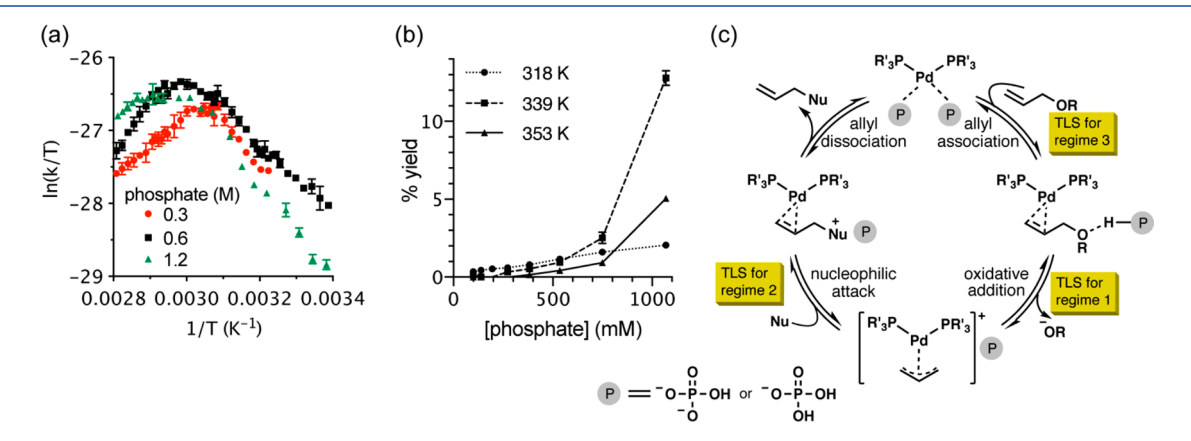


Figure 4. (a) Eyring plot with various phosphate concentrations. Conditions: 12.5 μ M APE, 9.4 nM Pd(NO₃)₂, 120 μ M TFP, 10 mM NaBH₄, 5% v/v DMSO/0.3, 0.6, or 1.2 M phosphate pH 7 buffer, 293–358 K, n = 4, 30 min. The raw data and the ΔH^{\ddagger} values are available in Tables S7 and S8 in the Supporting Information, respectively. (b) Phosphate concentration dependence. Conditions: 12.5 μ M APE, 5 nM Pd(NO₃)₂, 80 μ M TFP, 5% v/v DMSO/100–1070 mM phosphate pH 7 buffer, n = 3, 30 min. The raw data are available in Table S9 in the Supporting Information. (c) Working hypothesis for the roles of phosphate ions.

Hydrogen-bond-driven activation of allylic ethers has been previously reported in methanol.²¹ DFT calculations showed that hydrogen bonding could lower the activation energy by more than 20 kcal/mol.²¹

In the oxidative addition step, the counteranion may be rapidly exchanged from the phenolic oxide anion to a phosphate ion (Figure 4c). In the next step, because the nucleophile is a neutral species as we discuss later, a phosphate ion can lower the transition state energy by forming an ion pair with the incipient positive charge on the nucleophile. This would account for the phosphate-mediated acceleration of the deallylation in regime 2.

The palladium—phosphine binding can be reversible;^{74–76} thus, we asked whether phosphate ions could act as a competitive ligand against TFP toward palladium. As Figure S2 in the Supporting Information shows, lowering the phosphate concentration did not change the optimal concentration of TFP, indicating that these two species are probably not competing as palladium ligands.

Effect of NaBH₄ Concentration. The reduction of palladium(II) with >10 mM NaBH₄ is not the TLS because the deallylation rate was independent of NaBH₄ concentration. Little was known about the energetic contributions of NaBH₄ below 10 mM. With 12.5 μ M APE (Figure 5a and

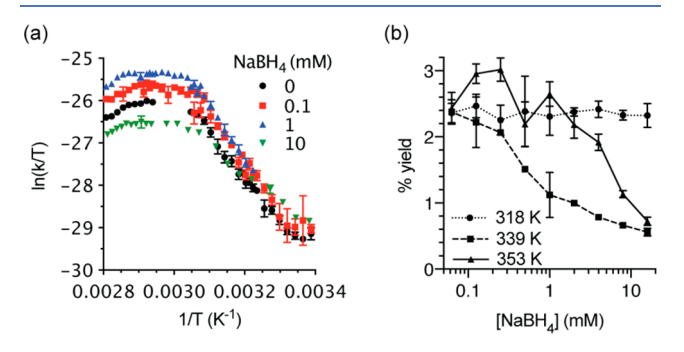


Figure 5. Various NaBH₄ concentrations. (a) Eyring plots. Conditions: 9.4 nM Pd(NO₃)₂, 120 μ M TFP, 0–10 mM NaBH₄, 5% v/v DMSO/1.2 M phosphate pH 7 buffer, 293–358 K, 30 min, n=5. The raw data are available in Table S10 in the Supporting Information. (b) NaBH₄ concentration dependence. Conditions: 0–16 mM NaBH₄, 12.5 μ M APE, 60 μ M TFP, 10 nM Pd(NO₃)₂, 5% v/v DMSO/1.2 M phosphate pH 7 buffer, 60 min, n=3. The raw data are available in Table S12 in the Supporting Information.

Table S11), the Eyring plots were similar in the 0–10 mM NaBH₄ concentration range. To understand the effect of NaBH₄ concentrations, we focused on three temperatures (318, 339, and 353 K) corresponding to regimes 1, 2, and 3. As Figure 5b shows, in regime 1 (318 K), the concentrations of NaBH₄ had no effect on the kinetics of the deallylation reaction. In regimes 2 and 3, higher concentrations of NaBH₄ retarded the reaction. Although it is unclear how NaBH₄ does so, it has become evident that NaBH₄ is probably not involved in TLSs in any regimes. The insights from these experiments may be applicable to synthetic organic chemistry, chemosensing, and bioorthogonal chemistry, in which NaBH₄ cannot be used.

Effect of Pd Concentration. Fluorescence was measured at 0–9.4 nM Pd concentrations (Figure 6a). The yields after 30 min under the three regimes were linearly proportional to Pd concentration (i.e., first order with respect to Pd concentration), indicating that catalytically active palladium species involved in TLSs are most likely monomeric. However, we acknowledge that the current high-throughput protocol is not compatible with the measurement of product formation with higher concentrations of palladium; with more palladium, nonlinear behavior may be observed.

Effect of Substrate Concentration. The rate of the reaction was investigated at different APE concentrations (3–48 μ M) (Figure 6b,c). The substrate concentration was linearly correlated with the percent yield under all regimes, suggesting that all of the TLSs involve the substrate in the transition state, as the general catalytic cycle indicates. It is possible that the linearity may be limited to the 3–48 μ M APE range, because Michaelis–Menten kinetics are still plausible at higher concetrations. To Unfortunately, the APE concentration range could not be broadened under the current conditions with 5% DMSO due to limited solubility.

Effect of DMSO Concentration. DMSO has been used as a cosolvent in aqueous palladium-catalyzed reactions to solubilize hydrophobic reactants. Because DMSO could bind to palladium, we wondered whether DMSO could affect the deallylation rate. Figure 7a shows the benchmark Eyring plot with 12.5 μ M APE in 5% DMSO (for quantitative data, see Table S16 in the Supporting Information). When 10% DMSO was used instead, regime 2 disappeared. The arrows indicate that DMSO decelerates and accelerates the deallylation above and below the first $T_{\rm inv}$ value, respectively.

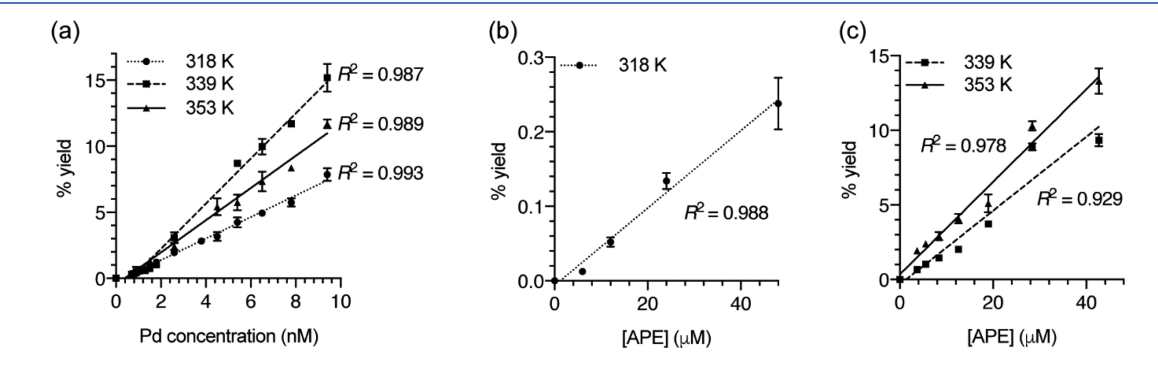


Figure 6. (a) Palladium concentration dependence. Conditions: 0-9.4 nM Pd(NO₃)₂,10 mM NaBH₄, 12.5μ M APE, 60μ M TFP, 5% v/v DMSO/1.23 M phosphate pH 7 buffer, $30 \min$, n = 4. The raw data are available in Table S13 in the Supporting Information. (b, c) APE concentration dependence. Conditions: $3-48 \mu$ M APE, 10μ nM Pd(NO₃)₂, 10μ M NaBH₄, 60μ M TFP, $5\% \nu$ v DMSO/1.23 M phosphate pH 7 buffer, 60μ M in the Supporting Information.

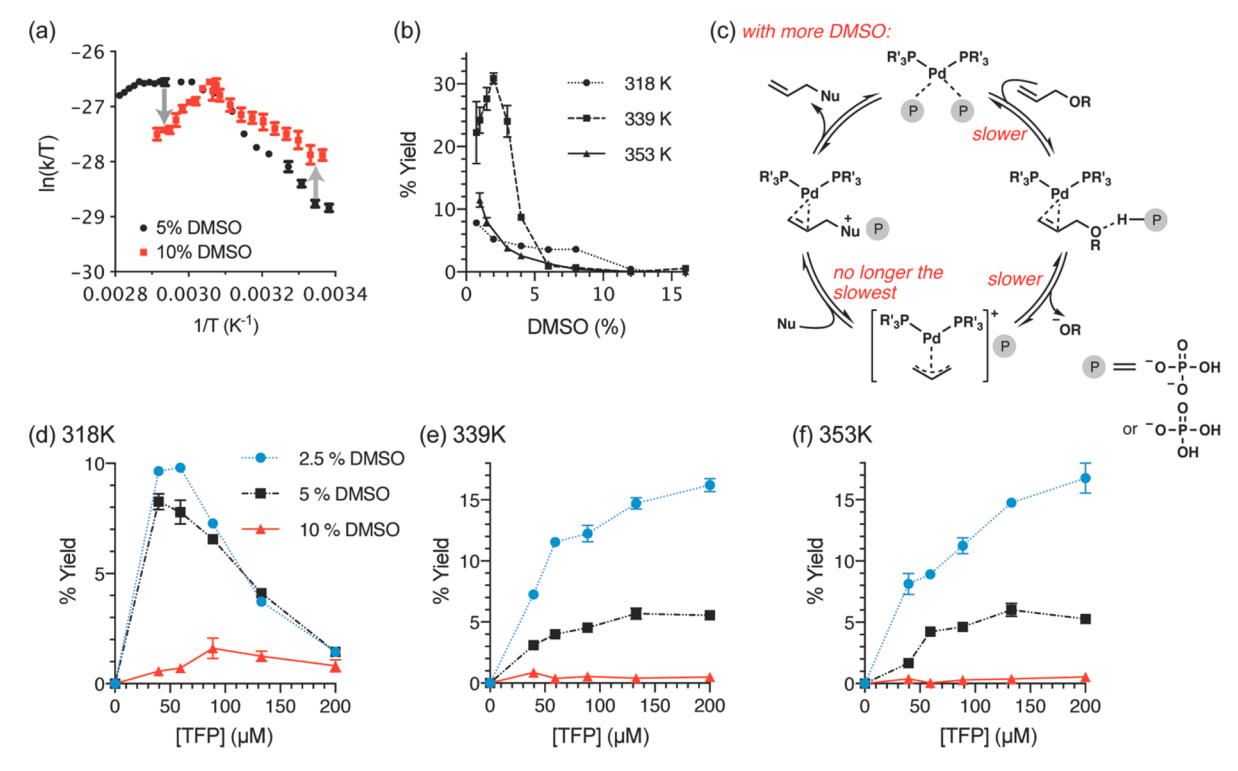


Figure 7. Various DMSO concentrations. (a) Conditions: 9.4 nM Pd(NO₃)₂, 12.5 μ M APE,120 μ M TFP, 10 mM NaBH₄, 5% v/v DMSO/1.2 M phosphate pH 7 buffer, 293–358 K, n=3 or 5. The raw data are available in Table S15 in the Supporting Information. (b) Conditions: 0.75–16% v/v DMSO/1.2 M phosphate pH 7 buffer, 10 mM NaBH₄, 12.5 μ M APE, 60 μ M TFP, 10 nM Pd(NO₃)₂, 60 min, n=4. The raw data are available in Table S17 in the Supporting Information. (c) Summary of the DMSO effect. Effect of DMSO on TFP–palladium binding. (d–f) Conditions: 0–200 μ M TFP, 10 nM Pd(NO₃)₂, 10 mM NaBH₄, 10 μ M APE, 2.5–10% v/v DMSO/1.1 M phosphate pH 7 buffer, 30 min. n=3. The raw data are available in Table S18 in the Supporting Information.

We titrated DMSO under regime 1 (318 K), regime 2 (339 K), and regime 3 (353 K) with 12.5 μ M APE (Figure 7b). Generally, high DMSO concentrations slowed the kinetics of deallylation under all regimes. Regime 2 was the most sensitive to DMSO concentration, with an optimal concentration of 2%. The positive correlation with up to 2% DMSO in regime 2 may require further studies to understand. Nonetheless, these results suggest that regime 2 is probably not a transition between regimes 1 and 3. Figure 7c summarizes the findings in Figure 7a,b.

If DMSO acts as a ligand in the current system, the optimal concentrations of TFP should be higher with more DMSO. Indeed, this was the case in regime 1 (Figure 7d), indicating that DMSO may act as a competitive ligand in the oxidative addition step to reversibly generate a resting species. The rate of deallylation for regimes 2 and 3 (Figure 7e,f) was very slow with 10% DMSO, making it difficult to determine the optimal TFP concentration. With 5% DMSO, the rate of the reaction started to decline as the TFP concentration reached 200 μ M at both 339 and 353 K. No decline in reactivity was observed with 2.5% DMSO at these temperatures. At this point, the role of DMSO in regimes 2 and 3 is not clear.

How does the higher concentration of DMSO decelerate the TLS of regime 3 by increasing the entropic penalty, as indicated by the arrow in Figure 7a? Our working hypothesis is that the alkene substrate and the catalyst may be more solvated by DMSO, requiring a greater loss of entropy to associate with each other (for the solvation of hydrophobic molecules in DMSO—water mixtures, see the work by the Bagchi group 81,82). Although DMSO accelerates the η^1 – η^3 isomerization in a phosphine-free system, 83 it is not clear whether the

phosphine-free system is relevant to the current system. Regardless, this result indicates that a rational approach toward accelerating a bioorthogonal Tsuji—Trost reaction may be to minimize the solvation of substrates and catalysts, for example, by exploiting hydrophobic effects, to facilitate the association of the two species under highly diluted conditions.

Competition Experiment. If the association of palladium species to the olefin is the slowest step in the catalytic cycle under regime 3, the presence of an external alkene should compete for the palladium, retarding the reaction. On the basis of this hypothesis, competition experiments under regimes 1, 2, and 3 were performed (Figure 8) with 12.5 μ M APE in the

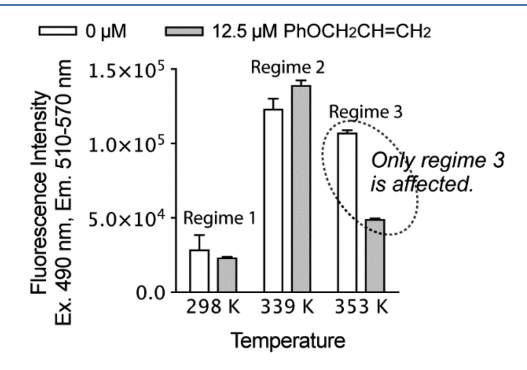


Figure 8. Competition experiments with APE and external alkene. Conditions: 0 or 12.5 μ M phenyl allyl ether, 12.5 μ M APE, 9.4 nM Pd(NO₃)₂, 120 μ M TFP, 10 mM NaBH₄, 5% DMSO/1.23 M phosphate pH 7 buffer, n = 3, 30 min. The raw data are available in Table S19 in the Supporting Information.

presence and absence of 12.5 μ M phenyl allyl ether. No change in fluorescence was observed under regimes 1 and 2 upon addition of the external alkene. Under regime 3, however, the rate of the reaction decreased by half in the presence of the alkene. These results support our hypothesis that association is the TLS in regime 3.

Identification of the Nucleophile. To model the reaction with density functional theory (DFT) calculations, we needed to identify the nucleophile of the reaction. Previous investigations revealed that the phosphate ions were not the nucleophiles. Spurred on by this, we analyzed a reaction mixture by LC-MS. A peak corresponding to P-allylated TFP 1 (Figure 9) was found, indicating that TFP is the primary

Figure 9. Formation of P-allyl TFP.

nucleophile. This is similar to the precedence in the literature, in which Ph_3P was allylated under Tsuji—Trost reaction conditions. As such, we further investigated TFP as the reaction nucleophile through decreasing both APE and TFP simultaneously to mimic reaction progress (Figure 10). The "same-excess" models 45-87 would afford a single line if the TFP is acting as the nucleophile. In effect, each decreasing concentration of APE was paired with an equally lower concentration of TFP to mimic the reaction progressing under the assumption that TFP is the only nucleophile. If TFP is not consumed, the reactions with 60, 50, and 40 μ M TFP would show different rates, as indicated by Figure 3b. Further increasing the TFP concentration (120, 110, or 100 μ M) at the same APE concentrations afforded the same effect as shown in Figure 3b.

In the same-excess experiments, we found that, unlike the kinetic data in Figure 1, the reaction continued at the same rate instead of slowing down over time (Figure 10). To investigate this seemingly contradictory result, we prepared an Eyring plot with the increased $Pd(NO_3)_2$ concentrations (3.6 μ M instead of 9.4 nM; Figure 11 and Table S22). The higher $Pd(NO_3)_2$

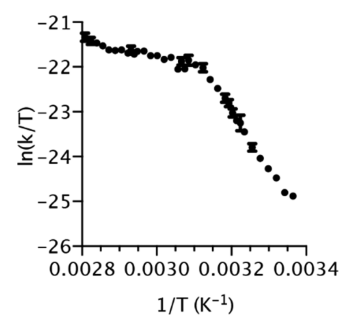


Figure 11. Eyring plot with increased palladium. Conditions: $3.6 \mu M$ Pd Pd(NO₃)₂, $12.5 \mu M$ APE, $120 \mu M$ TFP, 10 mM NaBH_4 , 5% v/v DMSO/1.23 M phosphate pH 7 buffer, 295-357 K, 30 min, n=4 or 5. The raw data are available in Table S22 in the Supporting Information.

concentration eliminated regime 3 at high temperatures, because the 400-fold higher concentration of palladium would lower the entropic penalty for the alkene association. It is noteworthy that the higher palladium concentration increased the ΔH^{\ddagger} value from 55 \pm 2 to 94 \pm 2 kJ/mol in the 293–326 K range.

Density Functional Theory Calculations. DFT calculations were performed to provide further insights into the TLSs of the palladium-catalyzed deallylation reaction (for previous computational studies of Tsuji—Trost-type reactions, see refs 21 and 88–91). The activation enthalpies and

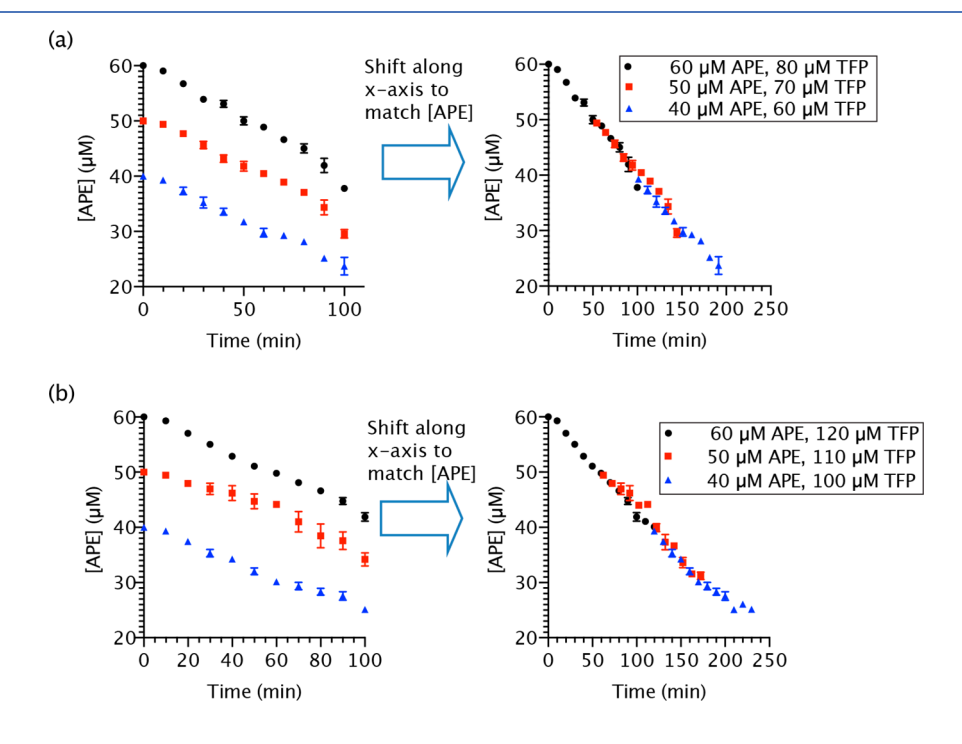


Figure 10. Same-excess experiments with TFP. On the right, graphs are adjusted to match the concentration of APE at given time points. (a, b) Conditions: $3.6 \,\mu\text{M} \,\text{Pd}(\text{NO}_3)_2$, $10 \,\text{mM} \,\text{NaBH}_4$, 5% v/v DMSO/1.23 M phosphate pH 7 buffer, 293 K, n=3. The data are available in Tables S20 and S21 in the Supporting Information.

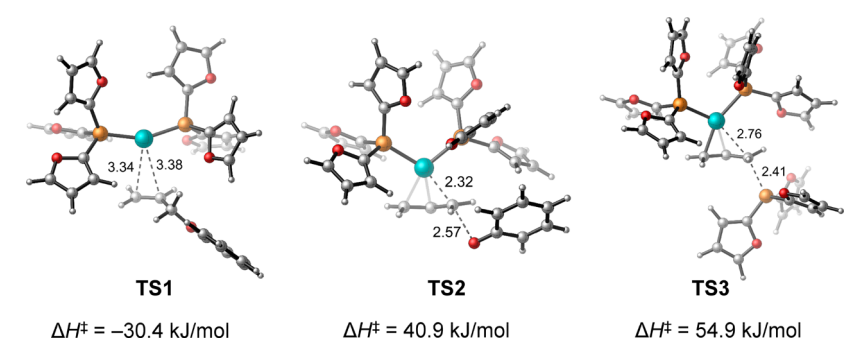


Figure 12. Optimized structures and activation energies of the transition states of allyl association (TS1), oxidative addition (TS2), and nucleophilic attack (TS3). The computed ΔH^{\ddagger} and ΔS^{\ddagger} values of TS1, TS2, and TS3 are with respect to Pd-1, Pd-2, and Pd-3, respectively (see Scheme 1). The data are available on page S21 in the Supporting Information.

entropies of three key steps of the reaction of allyl phenyl ether with the Pd(TFP)₂ catalyst were calculated using Gaussian 09 (see the Supporting Information for details). 92 The calculations were performed using B3LYP/LANL2DZ-6-31G(d) for geometry optimization and M06/SDD-6-311+G(d,p) for single-point energy calculations. Thermal corrections to the enthalpies and entropies were calculated using the gas-phase harmonic vibrational frequencies at 298 K. Solvation effects were taken into account in the single-point energy calculations using the SMD solvation model⁹³ and water as the solvent. A few possible nucleophiles were considered in the DFT calculations, including TFP, H₂PO₄⁻, and OH⁻. Among all the nucleophiles considered in the calculations, TFP has the lowest computed activation Gibbs free energies for the nucleophilic attack of the $(\pi$ -allyl)palladium intermediate (Figure 12), in agreement with the aforementioned experiments. The computed gas-phase ΔS^{\ddagger} values are expected to have large deviations from experimental data, 94 though the computed activation enthalpies (ΔH^{\ddagger}) of the three key steps in the catalytic cycle shed light on the experimentally proposed TLSs at different temperatures.

DFT calculations indicated that the allyl association step (TS1) is the most favorable enthalpically with a negative ΔH^{\dagger} (-30.4 kJ/mol), supporting the proposed assignment for the TLS of regime 3. Here, the activation enthalpy is calculated with respect to the separate reactants (the two-coordinated Pd(TFP)₂ catalyst, Pd-1, and the allyl phenyl ether). The negative activation enthalpy for this step is due to the exothermic formation of a van der Waals complex prior to the allyl association transition state (TS1) (see below for detailed discussions). The computed ΔH^{\ddagger} value of the oxidative addition step (TS2, 40.9 kJ/mol) is in reasonable agreement with the experimental value of 55 ± 2 kJ/mol measured at 293–326 K (regime 1). The nucleophilic attack of the $(\pi$ allyl)palladium complex by TFP (TS3) occurs via the outersphere pathway (Figure 12). The DFT calculations significantly overestimated the ΔH^{\ddagger} value of the nucleophilic attack (54.9 kJ/mol), in comparison to the experimental ΔH^{\dagger} value in regime 2 (326-347 K). The difference between the computational and experimental values is possibly due to the challenges of calculating solvation effects of the cationic (π allyl)palladium species, 95 as the DFT calculations and the experiments were performed in different media (water vs phosphate buffer) and the effects of the counteranion were not considered in the calculations. Taken together, the computational results support the hypothesis that three different TLSs are operating at different temperatures, although quantitative

prediction of ΔH^{\ddagger} in phosphate buffer solution remains challenging.

Detailed Mechanism of Allyl Association. The computed energy profile of the association of the allyl phenyl ether to the $Pd^0(TFP)_2$ complex (**Pd-1**) to form the π complex (**Pd-2**) is shown in Figure 13. The reaction first forms the van

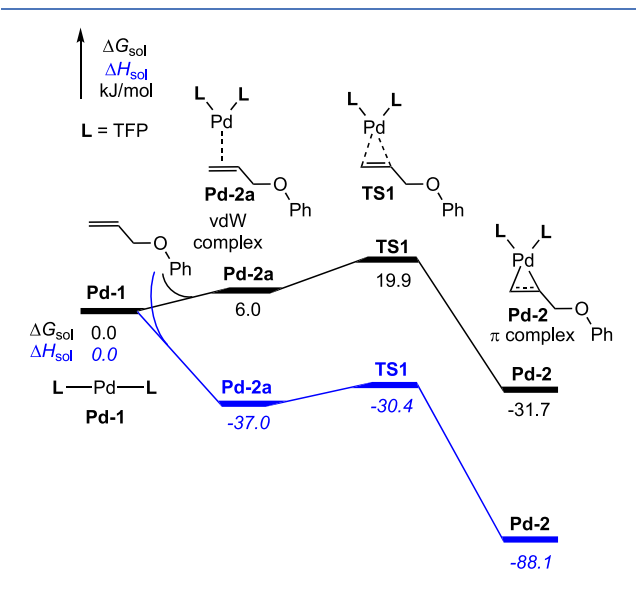


Figure 13. Computed energy profile of the association of the allyl phenyl ether to the $(TFP)_2Pd^0$ complex (Pd-1) to form the π complex (Pd-2).

der Waals (vdW) complex Pd-2a, which is 37.0 kJ/mol more stable than the separate reactants (Pd-1 and allyl phenyl ether) in terms of enthalpies. Due to entropic effects, this vdW complex is less stable than the separate reactants in terms of Gibbs free energies. It should be noted that, at the low concentrations in the present experimental study, the formation of the vdW complex is expected to be even less favorable. Thus, the resting state before the allyl association should be the separate reactants (Pd-1 and allyl phenyl ether), rather than the vdW complex Pd-2a. From the vdW complex, the association of the double bond in the allyl phenyl ether to the palladium to form the π complex Pd-2 occurs via TS1. The enthalpy of TS1 is 6.6 kJ/mol higher than that of the vdW complex and is 30.4 kJ/mol lower than that of the resting state (Pd-1). Thus, the overall enthalpy of activation of allyl association from Pd-1 to TS1 is negative ($\Delta H^{\dagger} = -30.4 \text{ kJ/}$ mol).

CONCLUSIONS

The sensitive and high-throughput fluorometric method allowed for measuring the activation enthalpy energies at micromolar concentrations of the substrate, revealing three regimes. The associated TLSs were assigned as oxidative addition (regime 1; $\Delta H^{\ddagger} > 0$), nucleophilic attack (regime 2; $\Delta H^{\ddagger} \approx 0$), and association (regime 3; $\Delta H^{\ddagger} < 0$). It is possible that regime 2 is a transition between regime 1 and regime 3, although our data support the existence of regime 2. The generality of the current findings must be examined in the future with other substrates and phosphines. Nonetheless, this work may provide kinetic insights into Tsuji-Trost reactions under biological or analytical conditions. For example, with a substrate and palladium at low micromolar to nanomolar concentrations, the TLS may be the association step. More broadly, the trend depicted in Figure 2b indicates that the kinetic profile can change from regime 1 to regime 2 and even to regime 3 as the substrate is consumed. It also suggests that the reaction may proceed in different regimes at different temperatures. Thus, a blueprint for developing a faster allylic C-O bond cleavage may be to determine the regime under which the reaction operates in order to rationally optimize the reaction conditions accordingly.

EXPERIMENTAL SECTION

Stock Solutions. Solutions of APE in DMSO were prepared and stored in amber bottles at 25 °C for up to 6 months. All the TFP solutions in DMSO used in this study were stabilized by 500 or 250 ppm butylated hydroxytoluene (BHT) and stored in amber bottles at 25 °C for >6 months without decomposition. Palladium solutions were prepared by diluting a high-purity palladium standard for atomic absorption spectroscopy (9.4 mM in 10% nitric acid) with 5% TraceMetal nitric acid in ultrapure water immediately prior to use (within 6 h).

Reagents. Water in this study was purified by a Barnstead Nanopure Diamond Lab Water System and distilled. Nitric acid was TraceMetal grade. DMSO was used without purification.

Instrumentation. All fluorescence measurements (excitation 490 nm, emission 510–570 nm) were carried out using a Promega Biosystems Modulus II Microplate Reader. Temperature increments were set using an Eppendorf Mastercycler Gradient PCR thermocycler. A temperature increment was applied, with median autocycler temperatures of 30, 45, 60, and 75 °C to span 20–85 °C (for example, 20, 23, 26, 29, 32, 35, and 38 °C for one experiment and 35, 38, 41, 44, 47, 50, and 53 °C for another experiment).

Measuring Consumption of APE (Figure 1). Phosphate pH 7 buffer (1.23 M; 9 mL), 0.2, 1.0, or 2.0 mM APE in DMSO (250 μ L), DMSO (500 μ L), and 3.2 mM TFP in DMSO (250 μ L) were combined in separate scintillation vials. The resulting solutions were cooled to 0 °C on ice and treated with 500 μ M Pd(NO₃)₂ in 5% TraceMetal HNO₃ (20 μ L) and 2.5 M NaBH₄ in 10 N NaOH (40 μ L). These solutions were warmed to room temperature to start the deallylation. Aliquots (20 μ L) of the solution were transferred to a black 96-well plate containing 1.2 M phosphate pH 7 buffer (180 μ L per well) every 3 min for 21 min, followed by every 10 min for 200 min for a total of 221 min. The fluorescence was measured. Moles of Pittsburgh Green were calculated according to our previous work (y = 124886x + 511, where x = Pittsburgh

Green concentration in μM and y = fluorescence intensity in arbitrary units from the instrument ⁹⁶) and used to measure the product formation. The amount of remaining APE was calculated by subtracting the amount of Pittsburgh Green produced from the initial concentration of APE.

General Procedure for Eyring Plot Preparation. The reaction solution on ice (200 μ L; preparation described above) was transferred to a 200 μL thin-walled PCR tube, which was capped and placed in the thermocycler with four replicates per temperature. A 3 K temperature increment was applied, with a median temperature as indicated, spanning a 20 K range. For example, for the data shown in Figure 2a, four reactions were set at 295.6, 299.0, 302.3, 305.7, 310.6, 314.0, 317.3, 320.7, 325.6, 329.0, 332.3, or 335.6 K, and the average and standard deviation were shown for each specific temperature. In the next experiment, the reactions were performed at 325.6, 329.0, 332.3, 335.6 340.7, 342.3, 344.0, 345.6, 347.3, 349.0, 350.6, and 352.3 K so that there is an overlap at 325.6, 329.0, 332.3, and 335.6 K. If the overlapped range showed discrepancy, we repeated the experiment until the overlap was acceptable for normalization. After the indicated time for each experiment, the PCR tubes were removed from the thermocycler and cooled to 0 °C on ice, and each solution (180 µL) was transferred to a black 96-well plate to measure fluorescence. Moles of Pittsburgh Green were calculated according to the method described above. The natural log of the rate against the inverse of the temperature was plotted to afford an Eyring plot for each condition tested. Data were plotted and analyzed using GraphPad Prism 8.1.2.

Eyring Plot with 12.5–50 μM APE(Figure 2a). Phosphate pH 7 buffer (1.23 M; 9.5 mL), 4.8 mM TFP in DMSO (250 μL), and 0.5, 1.0, or 2.0 mM APE in DMSO (250 μL) were combined in separate scintillation vials. The resulting solutions were cooled to 0 °C on ice. These solutions were treated with 4.7 μM Pd(NO₃)₂ in 5% TraceMetal HNO₃ (20 μL) and 2.5 M NaBH₄ in 10 N NaOH (40 μL). A temperature increment was applied for 30 min, with median autocycler temperatures of 30, 45, 60, and 75 °C to span 20–85 °C. The resulting reaction solutions were analyzed according to General Procedure for Eyring Plot Preparation (n = 3).

Eyring Plot with 60–240 μ M TFP (Figure 3a). Phosphate pH 7 buffer (1.23 M; 9.5 mL), 0.5 mM APE in DMSO (250 μ L), and 2.4, 4.8, or 9.6 mM TFP in DMSO (250 μ L) were combined in separate scintillation vials. These solutions were cooled to 0 °C on ice and treated with 4.7 μ M Pd(NO₃)₂ in 5% TraceMetal HNO₃ (20 μ L) and 2.5 M NaBH₄ in 10 N NaOH (40 μ L). A temperature increment was applied for 30 min, with median autocycler temperatures of 30, 45, 60, and 75 °C to span 20–85 °C. The resulting reaction solutions were analyzed according to General Procedure for Eyring Plot Preparation (n = 3).

TFP Concentration Dependence (Figure 3b). Phosphate pH 7 buffer (1.23 M; 15644 μ L), 800 μ M APE in DMSO (250 μ L), 9.4 μ M Pd(NO₃)₂ (16 μ L), 2.5 M NaBH₄ in 10 N NaOH (64 μ L), and DMSO (26.2 μ L) were combined in a scintillation vial. Aliquots (969 μ L per vial) of the resulting solution were transferred to 2 mL vials and cooled on ice. These aliquots were treated with 0, 0.322, 0.643, 0.965, 1.286, 1.608, 1.929, 2.251, 2.572, 2.894, 3.215, 3.537, 3.859, 4.180, or 4.502 mM TFP in DMSO (31 μ L). The resulting solutions were transferred to PCR tubes (200 μ L) and incubated at 45, 66, or 80 °C for 30 min. The resulting reaction solutions were

analyzed according to General Procedure for Eyring Plot Preparation (n = 3).

Eyring Plot with 0.3–1.2 M Phosphate lons (Figure 4a). Phosphate pH 7 buffer (0.3, 0.6, or 1.23 M; 9.5 mL), 0.5 mM APE in DMSO (250 μ L), and 4.8 mM TFP in DMSO (250 μ L) were combined in separate scintillation vials. The resulting solutions were cooled to 0 °C and treated with 4.7 μ M Pd(NO₃)₂ in 5% TraceMetal HNO₃ (20 μ L) and 2.5 M NaBH₄ in 10 N NaOH (40 μ L). A temperature increment was applied for 30 min, with median autocycler temperatures of 30, 45, 60, and 75 °C to span 20–85 °C. The resulting reaction solutions were analyzed according to General Procedure for Eyring Plot Preparation (n = 4).

Phosphate Concentration Dependence (Figure 4b). Phosphate pH 7 buffer (1.23 M; 4.08 mL), 500 μ M APE in DMSO (120 μ L), 3.2 mM TFP in DMSO (120 μ L), and 50 or 0 nM Pd(NO₃)₂ in 5% TraceMetal HNO₃ (480 μL) were mixed in a scintillation vial (solution A with palladium or solution B without pallladium). Water (18.764 mL), 235 μ M APE in DMSO (1.148 mL), 3.2 mM TFP in DMSO (540 μ L), and 94 nM Pd(NO₃)₂ in water (1148 μ L) were mixed in a scintillation vial (solution C). Water (19.912 mL), 235 µM APE in DMSO (1.148 mL), and 3.2 mM TFP in DMSO (540 μ L) were mixed in a scintillation vial (solution D). All resulting solutions were cooled to 0 $^{\circ}$ C on ice. Solution C (200 μ L) was added to wells rows A-D columns 2-7, and solution D (200 μ L) was added to wells rows E–H columns 2–7. Solution A (340 µL) was added to wells rows A-D column 1, and solution B (340 μ L) was added to wells rows E–H column 1 in a 96-well plate (1 mL per well). Serial dilutions (1.4-fold) were performed by mixing an aliquot (140 μ L) from wells in column 1 to wells in column 2, mixing, and continuing until wells in column 7 were mixed. The last 140 μ L was discarded from wells in column 7. Each solution in these wells was treated with 100 mM NaBH₄ in 10 N NaOH (20 μL) to prepare solutions with 10 mM NaBH₄. The resulting solutions were transferred to PCR tubes (200 μ L) and incubated at 45, 66, or 80 °C for 30 min. The resulting reaction solutions were analyzed according to General Procedure for Eyring Plot Preparation (n = 3).

Eyring pPlot with 0–10 mM NaBH₄ (Figure 5a). Phosphate pH 7 buffer (1.23 M; 9.5 mL), 0.5 or 2.0 mM APE in DMSO (250 μ L), and 4.8 mM TFP in DMSO (250 μ L) were combined in a scintillation vial. The resulting solutions were cooled to 0 °C and treated with 4.7 μ M Pd(NO₃)₂ in 5% TraceMetal HNO₃ (20 μ L) and 0, 0.025, 0.250, or 2.5 M NaBH₄ in 10 N NaOH (40 μ L). A temperature increment was applied for 30 min, with median autocycler temperatures of 30, 45, 60, and 75 °C to span 20–85 °C. The resulting reaction solutions were analyzed according to General Procedure for Eyring Plot Preparation (n = 5).

NaBH₄ Concentration Dependence (Figure 5b). Phosphate pH 7 buffer (1.2 M; 2.04 mL), 500 μM APE in DMSO (60 μL), 3.2 mM TFP in DMSO (60 μL), and 85 or 0 nM Pd(NO₃)₂ in 5% TraceMetal HNO₃ (240 μL) were mixed in a scintillation vial (solution E with palladium or solution F without palladium). Phosphate pH 7 buffer (1.23 M; 9.382 mL), 235 μM APE in DMSO (574 μL), 3.2 mM TFP in DMSO (270 μL), and 188 or 0 nM Pd(NO₃)₂ in 5% TraceMetal HNO₃ (574 μL) were mixed in a scintillation vial (solution G with palladium or solution H without palladium). All solutions were cooled to 0 °C on ice. Solution G (200 μL) was added to wells rows A–D columns 2–12 of a black 96-well

plate, and solution H (200 μ L) was added to wells rows E–H columns 2–12. Solution E (360 μ L) and 640 μ M NaBH₄ (40 μ L) in 10 N NaOH were added to wells rows A–D column 1. Solution F (360 μ L) and 640 μ M NaBH₄ (40 μ L) were added to wells rows E–H column 1. Twofold serial dilutions were performed by taking an aliquot (200 μ L) from wells in column 1, adding to wells in column 2, mixing, and continuing until wells in column 12 were mixed. The last 200 μ L was discarded from wells in column 12. The resulting solutions (200 μ L) were transferred to PCR tubes and incubated at 45, 66, or 80 °C for 60 min. The resulting reaction solutions were analyzed according to General Procedure for Eyring Plot Preparation (n = 3).

Pd Concentration Dependence (Figure 6a). Phosphate pH 7 buffer (1.23 M; 18.8 mL), 800 μ M APE in DMSO (348 μ L), 32 mM TFP in DMSO (83 μ L), 2.5 M NaBH₄ in 10 N NaOH (89 μ L), and DMSO (680 μ L) were mixed in a scintillation vial. An aliquot of the resulting solution (900 μ L) was treated with 0, 7, 9, 11, 13, 15, 18, 22, 26, 31, 38, 45, 54, 65, 78, or 94 nM Pd(NO₃)₂ in 5% TraceMetal HNO₃ (100 μ L). The resulting solutions were transferred to PCR tubes (230 μ L) and incubated at 45, 66, or 80 °C for 30 min. The resulting reaction solutions (230 μ L) were analyzed according to General Procedure for Eyring Plot Preparation (n = 3).

APE Concentration Dependence (Figure 6b,c). Phosphate pH 7 buffer (1.23 M; 2.04 mL), 2.56 mM APE in DMSO (60 μ L), 3.2 mM TFP in DMSO (60 μ L), and 85 or 0 nM Pd(NO₃)₂ in 5% TraceMetal HNO₃ (240 μ L) were mixed in a scintillation vial (solution I with palladium or solution I without palladium). Phosphate pH 7 buffer (1.23 M; 9.956 mL), 3.2 mM TFP in DMSO (270 μ L), and 188 or 0 nM $Pd(NO_3)_2$ in 5% TraceMetal HNO₃ (573.6 μ L) were mixed in a scintillation vial (solution K with palladium or solution L without palladium). All solutions were cooled to 0 °C on ice. Solution K (180 μ L) was added to wells rows A–D columns 2–8, and solution L (180 μ L) was added to wells rows E–H columns 2–8. Solution I (300 μ L) was added to wells rows A– D column 1, and solution J (300 μ L) was added to wells rows E-H column 1. Serial dilutions (1.5-fold) were performed by taking an aliquot (120 μ L) from wells in column 1, adding to wells in column 2, mixing, and continuing until wells in column 8 were mixed. The last 120 μ L was discarded from wells in column 8. Each well was treated with 100 mM NaBH4 in 10 N NaOH (20 μ L). The resulting solutions (200 μ L) were transferred to PCR tubes and incubated at 45, 66, or 80 °C for 30 min. The resulting reaction solution was analyzed according to General Procedure for Eyring Plot Preparation (n = 3).

Eyring Plot with 5 or 10% DMSO (Figure 7a). Phosphate pH 7 buffer (1.23 M; 9.50 mL), 500 μ M APE in DMSO (250 μ L), and 4.8 mM TFP in DMSO (250 μ L) were combined in a scintillation vial. In a separate scintillation vial, phosphate pH 7 buffer (1.23 M; 9.00 mL), 500 μ M APE in DMSO (250 μ L), 4.8 mM TFP in DMSO (250 μ L), and DMSO (500 μ L) were combined. All resulting solutions were cooled to 0 °C on ice and treated with 4.7 μ M Pd(NO₃)₂ in 5% TraceMetal HNO₃ (20 μ L) and 2.5 M NaBH₄ in 10 N NaOH (40 μ L). A temperature increment was applied for 30 min, with median autocycler temperatures of 30, 45, 65, °C to span 20–75 °C. The resulting reaction solution was analyzed according to General Procedure for Eyring Plot Preparation (n = 3 or 5).

Effect of DMSO Concentration (Figure 7b). Phosphate pH 7 buffer (1.23 M; 1.64 mL), 3.3 mM APE in DMSO (7.5

 μ L), 16, 9.6, 5.3, 3.7, 2.3, 1.7, 1.1, 0.787, 0.516, or 0.384 mM TFP in DMSO (312.5, 232.5, 152.5, 112.5, 72.5, 52.5, 32.5, 22.5, 12.5, or 7.5 μ L), and water (0, 80, 160, 200, 240, 260, 280, 290, 300, or 305 μ L) were combined in scintillation vials to prepare solutions (1.96 mL). These solutions (1.96 mL) were treated with 1.0 M NaBH₄ in 10 N NaOH (20 μ L) and 1.0 μ M Pd(NO₃)₂ in 5% TraceMetal HNO₃ (20 μ L). The reaction mixtures (200 μ L) were transferred to PCR tubes and incubated at 45, 60, or 80 °C for 60 min. The resulting reaction solution was analyzed according to General Procedure for Eyring Plot Preparation (n = 4).

Effect of DMSO on TFP-Palladium Binding (Figure 7d-f). Phosphate pH 7 buffer (1.10, 1.13, or 1.20 M; 6.615, 6.440, or 6.090 mL), DMSO (35, 210, 560 μ L), and 1 mM APE in DMSO (70 μ L) were combined in a scintillation vial. The resulting solutions (960 μ L) were treated with 500 mM NaBH₄ in 10 N NaOH (20 μ L) and 1 μ M Pd(NO₃)₂ in 5% TraceMetal HNO₃ (10 μ L) followed by 20, 13.3, 8.89, 5.93, or 3.95 mM TFP in DMSO (10 μ L). The resulting solutions were transferred to PCR tubes (230 μ L) and incubated at 45, 66, or 80 °C for 30 min. The resulting reaction solutions (200 μ L) were analyzed according to General Procedure for Eyring Plot Preparation (n = 3).

Competition Experiment (Figure 8). In two separate scintillation vials, phosphate pH 7 buffer (1.23 M; 945.1 μ L), 800 μ M APE in DMSO (15.6 μ L), 32 mM TFP in DMSO (3.75 μ L), and 2.5 M NaBH₄ in 10 N NaOH (4 μ L) were combined. The solution in vial 1 was diluted with DMSO (30.7 μ L). The solution in vial 2 was treated with 3.25 mM phenyl allyl ether in DMSO (3.9 μ L) and DMSO (26.8 μ L). The two solutions were treated with 10 μ M Pd(NO₃)₂ (0.94 μ L). The resulting solutions were transferred to PCR tubes (230 μ L) and incubated at 45, 66, or 80 °C for 30 min. The resulting reaction solutions (230 μ L) were analyzed according to General Procedure for Eyring Plot Preparation (n = 3).

Determination of TFP as Nucleophile Using "Same Excess" Measurements with Optimized TFP Conditions (Figure 10a). Phosphate pH 7 buffer (1.23 M; 1.9 mL), 2.4 mM APE in DMSO (50 μ L), and 3.2 mM TFP in DMSO (50 μ L) were combined in a scintillation vial to prepare a solution of 60 μ M APE and 80 μ M TFP. Phosphate pH 7 buffer (1.23) M; 1.9 mL), 2.0 mM APE in DMSO (50 μ L), and 2.8 mM TFP in DMSO (50 μ L) were combined to prepare a solution of 50 μ M APE and 70 μ M TFP. Phosphate pH 7 buffer (1.23 M; 1.9 mL), 1.6 mM APE in DMSO (50 μ L), and 2.4 mM TFP in DMSO (50 μ L) were combined to prepare a solution of 40 μ M APE and 60 μ M TFP. All resulting solutions were cooled to 0 °C on ice and treated with 180 μ M Pd(NO₃)₂ in 5% TraceMetal HNO₃ (40 μ L) and 500 mM NaBH₄ in 10 N NaOH (40 μ L). The resulting solutions were warmed to 24 °C to start the deally lation. At 10 min intervals, an aliquot (20 μ L) was transferred to phosphate pH 7 buffer (1.23 M; 180 μ L), and the resulting diluted solution was analyzed according to General Procedure for Eyring Plot Preparation (n = 3) to monitor the reactions for 120 min.

Determination of TFP as a Nucleophile Using "Same Excess" Measurements with Excess TFP Conditions (Figure 10b). Phosphate pH 7 buffer (1.23 M; 1.9 mL), 2.4 mM APE in DMSO (50 μ L), and 4.8 mM TFP in DMSO (50 μ L) were combined in a scintillation vial to prepare a solution of 60 μ M APE and 120 μ M TFP. Phosphate pH 7 buffer (1.23 M; 1.9 mL), 2.0 mM APE in DMSO (50 μ L), and 4.4 mM TFP in DMSO (50 μ L) were combined to prepare a solution

of 50 μ M APE and 110 μ M TFP. Phosphate pH 7 buffer (1.23 M; 1.9 mL), 1.6 mM APE in DMSO (50 μ L), and 4.0 mM TFP in DMSO (50 μ L) were combined to prepare a solution of 40 μ M APE and 100 μ M TFP. All resulting solutions were cooled to 0 °C on ice and treated with 180 μ M Pd(NO₃)₂ in 5% TraceMetal HNO₃ (40 μ L) and 500 mM NaBH₄ in 10 N NaOH (40 μ L). The resulting solutions were warmed to 24 °C to start the deallylation. At 10 min intervals, an aliquot (20 μ L) was transferred to 1.23 M phosphate pH 7 buffer (180 μ L), and the resulting diluted solution was analyzed according to General Procedure for Eyring Plot Preparation (n = 3) to monitor the reactions for 120 min.

Eyring Plot with 3.6 μ M Palladium (Figure 11). Phosphate pH 7 buffer (1.23 M; 9.5 mL), 800 μ M APE in DMSO (250 μ L), and 4.8 mM TFP in DMSO (250 μ L) were combined in a scintillation vial. The resulting solution was cooled to 0 °C on ice and treated with 1.8 mM Pd(NO₃)₂ in 5% TraceMetal HNO₃ (20 μ L) and 2.5 M NaBH₄ in 10 N NaOH (40 μ L). A temperature increment was applied for 30 min, with median autocycler temperatures of 30, 45, 60, and 75 °C to span 20–85 °C. The resulting reaction solutions were analyzed according to General Procedure for Eyring Plot Preparation (n = 4 or 5).

Effect of Phosphate lons on TFP–Palladium Binding (Figure S2). Phosphate pH 7 buffer (1.23 M; 18 mL) or phosphate pH 7 buffer (1.23 M; 7.32 mL) and water (10.68 mL) and 800 μM APE in DMSO (459 μL) were combined in a scintillation vial. Each solution (975 μL) was transferred to 2 mL Eppendorf tubes and treated with 0, 0.5, 1.0, 2.0, 4.0, or 8.0 mM TFP solutions in DMSO (25 μL). The resulting solutions were treated with 23.5 μM Pd(NO₃)₂ in 5% TraceMetal HNO₃ (20 μL;) and 500 mM NaBH₄ in 10 N NaOH (20 μL). The resulting reaction solution (200 μL) was transferred to a black 96-well fluorescence plate, and fluorescence was recorded initially and after incubation at 25 °C for 60 min. The resulting solutions (200 μL) were incubated at 45 °C for 60 min and analyzed according to General Procedure for Eyring Plot Preparation.

ASSOCIATED CONTENT

S Supporting Information

The Supporting Information is available free of charge at https://pubs.acs.org/doi/10.1021/acscatal.9b03011.

Additional kinetic data, raw data for figures in the main text, and computational details (PDF)

AUTHOR INFORMATION

Corresponding Authors

*E-mail for P.L.: pengliu@pitt.edu. *E-mail for K.K.: koide@pitt.edu.

ORCID

Matthew P. Tracey: 0000-0002-8015-9016

Peng Liu: 0000-0002-8188-632X

Kazunori Koide: 0000-0001-8894-8485

Author Contributions

[†]I.P. and M.P.T. contributed equally to this work.

Funding

This work was funded by US National Science Foundation Grants CHE-0911092 and CHE-1506942, the National Institutes of Health (R35GM128779), and the Wass Summer Research Fellowship (to M.J.L.). Calculations were performed

at the Center for Research Computing at the University of Pittsburgh and the Extreme Science and Engineering Discovery Environment (XSEDE) supported by the National Science Foundation.

Notes

The authors declare no competing financial interest.

ACKNOWLEDGMENTS

We thank Professor Donna Blackmond (The Scripps Research Institute) for suggesting the same-excess experiments.

REFERENCES

- (1) Trost, B. M.; Fullerto, Tj New Synthetic Reactions. Allylic Alkylation. J. Am. Chem. Soc. 1973, 95, 292–294.
- (2) Tsuji, J.; Takahash, H.; Morikawa, M. Organic Syntheses by Means of Noble Metal Compounds. 17. Reaction of Π-Allylpalladium Chloride with Nucleophiles. *Tetrahedron Lett.* **1965**, *6*, 4387–4388.
- (3) Trost, B. M.; VanVranken, D. L. Asymmetric Transition Metal-Catalyzed Allylic Alkylations. *Chem. Rev.* **1996**, *96*, 395–422.
- (4) Li, H. L.; Fan, J. L.; Peng, X. J. Colourimetric and Fluorescent Probes for the Optical Detection of Palladium Ions. *Chem. Soc. Rev.* **2013**, *42*, 7943–7962.
- (5) Koide, K., Palladium Detection Techniques for Active Pharmaceutical Ingredients Prepared *Via* Cross-Couplings. In *New Trends in Cross-Coupling: Theory and Applications*; Colacot, T. J., Ed.; Royal Society of Chemistry: 2015.
- (6) Tracey, M. P.; Pham, D.; Koide, K. Fluorometric Imaging Methods for Palladium and Platinum and the Use of Palladium for Imaging Biomolecules. *Chem. Soc. Rev.* **2015**, *44*, 4769–4791.
- (7) Tan, H. Y.; Liu, J. G.; Zhou, L. F.; Li, Y. K.; Yan, J. W.; Zhang, L. A Smart Nir Fluorescent Probe for the Highly Selective Detection of Palladium. *RSC Adv.* **2017**, *7*, 6583–6586.
- (8) Yan, J. W.; Wang, X. L.; Zhou, L. F.; Zhang, L. Cv-Apc, a Colorimetric and Red-Emitting Fluorescent Dual Probe for the Highly Sensitive Detection of Palladium. *RSC Adv.* **2017**, *7*, 20369–20372.
- (9) Feng, W. Y.; Bai, L. Y.; Jia, S. W.; Feng, G. Q. A Novel Phthalimide-Rhodol-Based ESIPT-FRET System for Rapid Colorimetric and Ratiometric Fluorescent Detection of Palladium. *Sens. Actuators, B* **2018**, 260, 554–562.
- (10) Baker, M. S.; Phillips, S. T. A Two-Component Small Molecule System for Activity-Based Detection and Signal Amplification: Application to the Visual Detection of Threshold Levels of Pd(II). *J. Am. Chem. Soc.* **2011**, *133*, 5170–5173.
- (11) Chankeshwara, S. V.; Indrigo, E.; Bradley, M. Palladium-Mediated Chemistry in Living Cells. *Curr. Opin. Chem. Biol.* **2014**, 21C, 128–135.
- (12) Luo, W. F.; Li, J.; Liu, W. S. A Two-Photon Ratiometric ESIPT Probe for Fast Detection and Bioimaging of Palladium Species. *Org. Biomol. Chem.* **2017**, *15*, 5846–5850.
- (13) Su, W.; Gu, B.; Hu, X. J.; Duan, X. L.; Zhang, Y. Y.; Lie, H. T.; Yao, S. Z. A near-Infrared and Colorimetric Fluorescent Probe for Palladium Detection and Bioimaging. *Dyes Pigm.* **2017**, *137*, 293–298.
- (14) Kuhana, A. T.; Feng, W. Y.; Feng, G. Q. A Simple but Effective Colorimetric and Far-Red to near-Infrared Fluorescent Probe for Palladium and Its Application in Living Cells. *Dyes Pigm.* **2018**, *152*, 112–117.
- (15) Xia, Q. F.; Feng, S. M.; Liu, D. D.; Feng, G. Q. A Highly Selective and Sensitive Colorimetric and near-Infrared Fluorescent Turn-on Probe for Rapid Detection of Palladium in Drugs and Living Cells. Sens. Actuators, B 2018, 258, 98–104.
- (16) Jin, M.; Wei, L.; Yang, Y.; Run, M.; Yin, C. A New Turn-on Fluorescent Probe for the Detection of Palladium(0) and Its Application in Living Cells and Zebrafish. *New J. Chem.* **2019**, *43*, 548–551.

(17) Fairlamb, I. J. S.; Lloyd-Jones, G. C. On the Effect of Catalyst Loading in Pd-Catalysed Allylic Alkylation. *Chem. Commun.* **2000**, 2447–2448.

- (18) Agenet, N.; Amatore, C.; Gamez, S.; Gérardin, H.; Jutand, A.; Meyer, G.; Orthwein, C. Effect of the Leaving Group and the Allylic Structure on the Kinetics and Thermodynamics of the Reaction of Allylic Carboxylates with Palladium(0) Complexes. *Arkivoc* **2002**, 92–101.
- (19) Evans, L. A.; Fey, N.; Harvey, J. N.; Hose, D.; Lloyd-Jones, G. C.; Murray, P.; Orpen, A. G.; Osborne, R.; Owen-Smith, G. J. J.; Purdie, M. Counterintuitive Kinetics in Tsuji—Trost Allylation: Ion-Pair Partitioning and Implications for Asymmetric Catalysis. *J. Am. Chem. Soc.* **2008**, *130*, 14471—14473.
- (20) Sherden, N. H.; Behenna, D. C.; Virgil, S. C.; Stoltz, B. M. Unusual Allylpalladium Carboxylate Complexes: Identification of the Resting State of Catalytic Enantioselective Decarboxylative Allylic Alkylation Reactions of Ketones. *Angew. Chem., Int. Ed.* **2009**, *48*, 6840–6843.
- (21) Huo, X. H.; Yang, G. Q.; Liu, D. L.; Liu, Y. G.; Gridnev, I. D.; Zhang, W. B. Palladium-Catalyzed Allylic Alkylation of Simple Ketones with Allylic Alcohols and Its Mechanistic Study. *Angew. Chem., Int. Ed.* **2014**, *53*, *6776*–*6780*.
- (22) Shintani, R.; Tsuji, T.; Park, S.; Hayashi, T. Mechanistic Investigation of the Palladium-Catalyzed Decarboxylative Cyclization of Γ-Methylidene- Δ -Valerolactones with Isocyanates: Kinetic Studies and Origin of the Site Selectivity in the Nucleophilic Attack at a (Π-Allyl)Palladium. *J. Am. Chem. Soc.* **2010**, *132*, 7508–7513.
- (23) Katcher, M. H.; Norrby, P.-O.; Doyle, A. G. Mechanistic Investigations of Palladium-Catalyzed Allylic Fluorination. *Organometallics* **2014**, 33, 2121–2133.
- (24) DeAngelis, A. J.; Gildner, P. G.; Chow, R.; Colacot, T. J. Generating Active "L-Pd(0)" Via Neutral or Cationic Π-Allylpalladium Complexes Featuring Biaryl/Bipyrazolylphosphines: Synthetic, Mechanistic, and Structure Activity Studies in Challenging Cross-Coupling Reactions. *J. Org. Chem.* **2015**, *80*, 6794–6813.
- (25) Johansson Seechurn, C. C.; Sperger, T.; Scrase, T. G.; Schoenebeck, F.; Colacot, T. J. Understanding the Unusual Reduction Mechanism of Pd(II) to Pd(I): Uncovering Hidden Species and Implications in Catalytic Cross-Coupling Reactions. *J. Am. Chem. Soc.* **2017**, *139*, 5194–5200.
- (26) Balamurugan, R.; Liu, J. H.; Liu, B. T. A Review of Recent Developments in Fluorescent Sensors for the Selective Detection of Palladium Ions. *Coord. Chem. Rev.* **2018**, *376*, 196–224.
- (27) Miller, M. A.; Askevold, B.; Mikula, H.; Kohler, R. H.; Pirovich, D.; Weissleder, R. Nano-Palladium Is a Cellular Catalyst for *in Vivo* Chemistry. *Nat. Commun.* **2017**, *8*, 15906.
- (28) Garner, A. L.; Song, F. L.; Koide, K. Enhancement of a Catalysis-Based Fluorometric Detection Method for Palladium through Rational Fine-Tuning of the Palladium Species. *J. Am. Chem. Soc.* **2009**, *131*, 5163–5171.
- (29) Koide, K.; Tracey, M. P.; Bu, X.; Jo, J.; Williams, M. J.; Welch, C. J. A Competitive and Reversible Deactivation Approach to Catalysis-Based Quantitative Assays. *Nat. Commun.* **2016**, *7*, 10691.
- (30) Nieberding, M.; Tracey, M. P.; Koide, K. Noneffervescent Method for Catalysis-Based Palladium Detection with Color or Fluorescence. *ACS Sens.* **2017**, *2*, 1737–1743.
- (31) Bu, X.; Williams, M.; Jo, J.; Koide, K.; Welch, C. J. Online Sensing of Palladium in Flowing Streams. *Chem. Commun.* **2017**, *53*, 720–723.
- (32) Yusop, R. M.; Unciti-Broceta, A.; Johansson, E. M. V.; Sanchez-Martin, R. M.; Bradley, M. Palladium-Mediated Intracellular Chemistry. *Nat. Chem.* **2011**, *3*, 239–243.
- (33) Li, J.; Yu, J. T.; Zhao, J. Y.; Wang, J.; Zheng, S. Q.; Lin, S. X.; Chen, L.; Yang, M. Y.; Jia, S.; Zhang, X. Y.; Chen, P. R. Palladium-Triggered Deprotection Chemistry for Protein Activation in Living Cells. *Nat. Chem.* **2014**, *6*, 352–361.
- (34) Weiss, J. T.; Dawson, J. C.; Fraser, C.; Rybski, W.; Torres-Sanchez, C.; Bradley, M.; Patton, E. E.; Carragher, N. O.; Unciti-

Broceta, A. Development and Bioorthogonal Activation of Palladium-Labile Prodrugs of Gemcitabine. *J. Med. Chem.* **2014**, *57*, 5395–5404.

- (35) Weiss, J. T.; Dawson, J. C.; Macleod, K. G.; Rybski, W.; Fraser, C.; Torres-Sánchez, C.; Patton, E. E.; Bradley, M.; Carragher, N. O.; Unciti-Broceta, A. Extracellular Palladium-Catalysed Dealkylation of 5-Fluoro-1-Propargyl-Uracil as a Bioorthogonally Activated Prodrug Approach. *Nat. Commun.* **2014**, *5*, 3277.
- (36) Weiss, J. T.; Carragher, N. O.; Unciti-Broceta, A. Palladium-Mediated Dealkylation of *N*-Propargyl-Floxuridine as a Bioorthogonal Oxygen-Independent Prodrug Strategy. *Sci. Rep.* **2015**, *5*, 9329.
- (37) Coelho, S. E.; Schneider, F. S. S.; de Oliveira, D. C.; Tripodi, G. L.; Eberlin, M. N.; Caramori, G. F.; de Souza, B.; Domingos, J. B. Mechanism of palladium(II)-Mediated Uncaging Reactions of Propargylic Substrates. *ACS Catal.* **2019**, *9*, 3792–3799.
- (38) Song, F. L.; Garner, A. L.; Koide, K. A Highly Sensitive Fluorescent Sensor for Palladium Based on the Allylic Oxidative Insertion Mechanism. *J. Am. Chem. Soc.* **2007**, *129*, 12354–12355.
- (39) Koide, K.; Song, F. L.; de Groh, E. D.; Garner, A. L.; Mitchell, V. D.; Davidson, L. A.; Hukriede, N. A. Scalable and Concise Synthesis of Dichlorofluorescein Derivatives Displaying Tissue Permeation in Live Zebrafish Embryos. *ChemBioChem* **2008**, *9*, 214–218.
- (40) Yang, Y. W.; Unsworth, L. D.; Semagina, N. Size- and Shape-Controlled Palladium Nanoparticles in a Fluorometric Tsuji—Trost Reaction. *J. Catal.* **2011**, 281, 137—146.
- (41) Garner, A. L.; Koide, K. Studies of a Fluorogenic Probe for Palladium and Platinum Leading to a Palladium-Specific Detection Method. *Chem. Commun.* **2009**, 86–88.
- (42) Song, F. L.; Carder, E. J.; Kohler, C. C.; Koide, K. Studies toward an Ideal Fluorescence Method to Measure Palladium in Functionalized Organic Molecules: Effects of Sodium Borohydride, Temperature, Phosphine Ligand, and Phosphate Ions on Kinetics. *Chem. Eur. J.* **2010**, *16*, 13500–13508.
- (43) Racys, D. T.; Eastoe, J.; Norrby, P. O.; Grillo, I.; Rogers, S. E.; Lloyd-Jones, G. C. Pd-H³-C₆H₉ Complexes of the Trost Modular Ligand: High Nuclearity Columnar Aggregation Controlled by Concentration, Solvent and Counterion. *Chem. Sci.* **2015**, *6*, 5793–5801
- (44) Hale, K. J.; Ridd, H. J. A Reassessment of the Isoinversion Relationship. *J. Chem. Soc., Perkin Trans.* 2 1995, 1601–1605.
- (45) Hale, K. J.; Ridd, J. H. A Reassessment of the Isoinversion Principle. J. Chem. Soc., Chem. Commun. 1995, 357–358.
- (46) Brown, K. L.; Li, J. Activation Parameters for the Carbon-Cobalt Bond Homolysis of Coenzyme B₁₂ Induced by the B₁₂-Dependent Ribonucleotide Reductase from *Lactobacillus Leichmannii*. *J. Am. Chem. Soc.* **1998**, *120*, 9466–9474.
- (47) Valentine, A. M.; Stahl, S. S.; Lippard, S. J. Mechanistic Studies of the Reaction of Reduced Methane Monooxygenase Hydroxylase with Dioxygen and Substrates. *J. Am. Chem. Soc.* **1999**, *121*, 3876–3887.
- (48) Simões, J. A. M.; Beauchamp, J. L. Transition-Metal Hydrogen and Metal-Carbon Bond Strengths: The Keys to Catalysis. *Chem. Rev.* **1990**, *90*, *629*–*688*.
- (49) Houk, K. N.; Rondan, N. G.; Mareda, J. Theoretical Studies of Halocarbene Cycloaddition Selectivities a New Interpretation of Negative Activation Energies and Entropy Control of Selectivity. *Tetrahedron* 1985, 41, 1555–1563.
- (50) Moss, R. A.; Lawrynowicz, W.; Turro, N. J.; Gould, I. R.; Yuan, C. Activation Parameters for the Additions of Arylhalocarbenes to Alkenes. *J. Am. Chem. Soc.* **1986**, *108*, 7028–7032.
- (51) Benson, S. W.; Dobis, O. Existence of Negative Activation Energies in Simple Bimolecular Metathesis Reactions and Some Observations on Too-Fast Reactions. *J. Phys. Chem. A* **1998**, *102*, 5175–5181.
- (52) Mozurkewich, M.; Benson, S. W. Negative Activation Energies and Curved Arrhenius Plots. 1. Theory of Reactions over Potential Wells. *J. Phys. Chem.* **1984**, *88*, 6429–6435.

- (53) Mozurkewich, M.; Lamb, J. J.; Benson, S. W. Negative Activation Energies and Curved Arrhenius Plots. 2. OH + CO. *J. Phys. Chem.* **1984**, 88, 6435–6441.
- (54) Shimomura, T.; Tölle, K. J.; Smid, J.; Szwarc, M. Energy and Entropy of Activation of Propagation by Free Polystyryl Anions and Their Ion Pairs. Phenomenon of Negative Activation Energy. *J. Am. Chem. Soc.* **1967**, *89*, 796–803.
- (55) Heller, D.; Buschmann, H.; Neumann, H. Conditions for Maxima and Minima as Inversion Points in the Temperature Dependence of Selection Processes. *J. Chem. Soc., Perkin Trans.* 2 1999, 175–181.
- (56) Olson, L. P.; Kuwata, K. T.; Bartberger, M. D.; Houk, K. N. Conformation-Dependent State Selectivity in O-O Cleavage of ONOONO: An "Inorganic Cope Rearrangement" Helps Explain the Observed Negative Activation Energy in the Oxidation of Nitric Oxide by Dioxygen. J. Am. Chem. Soc. 2002, 124, 9469–9475.
- (57) Rosokha, S. V.; Kochi, J. K. The Preorganization Step in Organic Reaction Mechanisms. Charge-Transfer Complexes as Precursors to Electrophilic Aromatic Substitutions. *J. Org. Chem.* **2002**, *67*, 1727–1737.
- (58) Erden, I.; Alscher, P. E.; Keeffe, J. R.; Mercer, C. Dye-Sensitized Photooxygenation of the C = N Bond. 5. Substituent Effects on the Cleavage of the C = N Bond of C-aryl-N-aryl-N-methylhydrazones. J. Org. Chem. 2005, 70, 4389–4392.
- (59) Han, X.; Lee, R.; Chen, T.; Luo, J.; Lu, Y. X.; Huang, K. W. Kinetic Evidence of an Apparent Negative Activation Enthalpy in an Organocatalytic Process. *Sci. Rep.* **2013**, *3*, No. e2557.
- (60) Zhu, X. Q.; Zhang, J. Y.; Cheng, J. P. Negative Kinetic Temperature Effect on the Hydride Transfer from NADH Analogue Bnah to the Radical Cation of *N*-benzylphenothiazine in Acetonitrile. *J. Org. Chem.* **2006**, *71*, 7007–7015.
- (61) Langhals, H.; Eberspächer, M.; Mayer, P. Uncatalyzed C-H Amination of Aromatic Compounds under Unusually Mild Conditions with Negative Enthalpies of Activation. *Asian J. Org. Chem.* **2017**, *6*, 1080–1085.
- (62) Ruiz-Castillo, P.; Blackmond, D. G.; Buchwald, S. L. Rational Ligand Design for the Arylation of Hindered Primary Amines Guided by Reaction Progress Kinetic Analysis. *J. Am. Chem. Soc.* **2015**, *137*, 3085–3092.
- (63) Martin, R.; Buchwald, S. L. Palladium-Catalyzed Suzuki-Miyaura Cross-Coupling Reactions Employing Dialkylbiaryl Phosphine Ligands. *Acc. Chem. Res.* **2008**, *41*, 1461–1473.
- (64) Niemeyer, Z. L.; Milo, A.; Hickey, D. P.; Sigman, M. S. Parameterization of Phosphine Ligands Reveals Mechanistic Pathways and Predicts Reaction Outcomes. *Nat. Chem.* **2016**, *8*, 610–617.
- (65) Farina, V.; Krishnan, B. Large Rate Accelerations in the Stille Reaction with Tri-2-Furylphosphine and Triphenylarsine as Palladium Ligands: Mechanistic and Synthetic Implications. *J. Am. Chem. Soc.* 1991, 113, 9585–9595.
- (66) Tymonko, S. A.; Smith, R. C.; Ambrosi, A.; Ober, M. H.; Wang, H.; Denmark, S. E. Mechanistic Significance of the Si-O-Pd Bond in the Palladium-Catalyzed Cross-Coupling Reactions of Arylsilanolates. *J. Am. Chem. Soc.* **2015**, *137*, 6200–6218.
- (67) Amatore, C.; Jutand, A.; Khalil, F. Neutral Palladium(0) Complexes from Pd(OAc)₂ and Tri-2-Furylphosphine and Their Reactivity in Oxidative Addition of Iodobenzene. *Arkivoc* **2006**, 38–48
- (68) Lo, J. C. L.; Gui, J. H.; Yabe, Y. K.; Pan, C. M.; Baran, P. S. Functionalized Olefin Cross-Coupling to Construct Carbon-Carbon Bonds. *Nature* **2014**, *516*, 343–348.
- (69) Calleja, J.; Pla, D.; Gorman, T. W.; Domingo, V.; Haffemayer, B.; Gaunt, M. J. A Steric Tethering Approach Enables Palladium-Catalysed C-H Activation of Primary Amino Alcohols. *Nat. Chem.* **2015**, *7*, 1009–1016.
- (70) Jiang, G.; List, B. Direct Asymmetric A-Allylation of Aldehydes with Simple Allylic Alcohols Enabled by the Concerted Action of Three Different Catalysts. *Angew. Chem., Int. Ed.* **2011**, *50*, 9471–9474.

(71) Tao, Z. L.; Zhang, W. Q.; Chen, D. F.; Adele, A.; Gong, L. Z. Pd-catalyzed Asymmetric Allylic Alkylation of Pyrazol-5-Ones with Allylic Alcohols: The Role of the Chiral Phosphoric Acid in C-O Bond Cleavage and Stereocontrol. *J. Am. Chem. Soc.* **2013**, *135*, 9255–9258.

- (72) El Maadi, A.; Bennazha, J.; Réau, J. M.; Boukhari, A.; Holt, E. M. New Palladium Phosphate Complexes: $K_2PdP_2O_7$ and $K_{3.5}Pd_{2.25}(P_2O_7)_2$ Synthesis, Single Crystal Structure and Conductivity. *Mater. Res. Bull.* **2003**, *38*, 865–874.
- (73) Lii, K.-H.; Wang, S.-L.; Liao, F.-L. $Cs_2Pd_3(P_2O_7)_2$ and $Cs_2Pd_3(As_2O_7)_2$: A 3D Palladium Phosphate with a Tunnel Structure and a 2D Palladium Arsenate Containing Strings of Palladium Atoms. *Inorg. Chem.* **2004**, *43*, 2499–2502.
- (74) Cai, S. T.; Lu, Y.; He, S.; Wei, F. F.; Zhao, L. C.; Zeng, X. S. A Highly Sensitive and Selective Turn-on Fluorescent Chemosensor for Palladium Based on a Phosphine-Rhodamine Conjugate. *Chem. Commun.* **2013**, 49, 822–824.
- (75) Yoshida, T.; Otsuka, S. Reactions of Two-Coordinate Phosphine Platinum(0) and Palladium(0) Compounds. Ligand Exchange and Reactivities toward Small Molecules. *J. Am. Chem. Soc.* 1977, 99, 2134–2140.
- (76) Ahlquist, M. S. G.; Norrby, P. O. Dispersion and Back-Donation Gives Tetracoordinate [Pd(PPh₃)₄]. *Angew. Chem., Int. Ed.* **2011**, *50*, 11794–11797.
- (77) Lukomski, L.; Pohorilets, I.; Koide, K. Third-Generation Method for High Throughput Quantification of Trace Palladium by Color or Fluorescence. *ChemRxiv* **2019**.
- (78) Wang, J.; Cheng, B.; Li, J.; Zhang, Z. Y.; Hong, W. Y.; Chen, X.; Chen, P. R. Chemical Remodeling of Cell-Surface Sialic Acids through a Palladium-Triggered Bioorthogonal Elimination Reaction. *Angew. Chem., Int. Ed.* **2015**, *54*, 5364–5368.
- (79) Diao, T. N.; White, P.; Guzei, I.; Stahl, S. S. Characterization of DMSO Coordination to palladium(II) in Solution and Insights into the Aerobic Oxidation Catalyst, Pd(DMSO)₂(TFA)₂. *Inorg. Chem.* **2012**, *51*, 11898–11909.
- (80) Drinkel, E. E.; Wu, L. L.; Linden, A.; Dorta, R. Synthesis, Structure, and Catalytic Studies of Palladium and Platinum Bis-Sulfoxide Complexes. *Organometallics* **2014**, *33*, 627–636.
- (81) Banerjee, S.; Roy, S.; Bagchi, B. Enhanced Pair Hydrophobicity in the Water-Dimethylsulfoxide (DMSO) Binary Mixture at Low DMSO Concentrations. *J. Phys. Chem. B* **2010**, *114*, 12875–12882.
- (82) Ghosh, R.; Banerjee, S.; Chakrabarty, S.; Bagchi, B. Anomalous Behavior of Linear Hydrocarbon Chains in Water-DMSO Binary Mixture at Low DMSO Concentration. *J. Phys. Chem. B* **2011**, *115*, 7612–7620.
- (83) Larsson, J. M.; Szabó, K. J. Mechanistic Investigation of the Palladium-Catalyzed Synthesis of Allylic Silanes and Boronates from Allylic Alcohols. *J. Am. Chem. Soc.* **2013**, *135*, 443–455.
- (84) Amatore, C.; Jutand, A.; M'Barki, M. A.; Meyer, G.; Mottier, L. Importance of the Presence of Chloride Ions in the First Steps of Palladium-Catalyzed Nucleophilic Allylic Substitutions. *Eur. J. Inorg. Chem.* **2001**, 2001, 873–880.
- (85) Mathew, J. S.; Klussmann, M.; Iwamura, H.; Valera, F.; Futran, A.; Emanuelsson, E. A. C.; Blackmond, D. G. Investigations of Pdcatalyzed ArX Coupling Reactions Informed by Reaction Progress Kinetic Analysis. *J. Org. Chem.* **2006**, *71*, 4711–4722.
- (86) O'Brien, A. G.; Luca, O. R.; Baran, P. S.; Blackmond, D. G. In Situ Ftir Spectroscopic Monitoring of Electrochemically Controlled Organic Reactions in a Recycle Reactor. *React. Chem. Eng.* **2016**, *1*, 90–95.
- (87) Blackmond, D. G. Reaction Progress Kinetic Analysis: A Powerful Methodology for Mechanistic Studies of Complex Catalytic Reactions. *Angew. Chem., Int. Ed.* **2005**, *44*, 4302–4320.
- (88) Piechaczyk, O.; Thoumazet, C.; Jean, Y.; Le Floch, P. DFT Study on the Palladium-Catalyzed Allylation of Primary Amines by Allylic Alcohol. *J. Am. Chem. Soc.* **2006**, *128*, 14306–14317.
- (89) Mora, G.; Piechaczyk, O.; Le Goff, X. F.; Le Floch, P. Palladium-Catalyzed Deallylation of Allyl Ethers with a Xanthene

Phosphole Ligand. Experimental and DFT Mechanistic Studies. Organometallics 2008, 27, 2565–2569.

- (90) De Luliis, M. Z.; Watson, I. D. G.; Yudin, A. K.; Morris, R. H. A DFT Investigation into the Origin of Regioselectivity in Palladium-Catalyzed Allylic Amination. *Can. J. Chem.* **2009**, *87*, 54–62.
- (91) Keith, J. A.; Behenna, D. C.; Sherden, N.; Mohr, J. T.; Ma, S.; Marinescu, S. C.; Nielsen, R. J.; Oxgaard, J.; Stoltz, B. M.; Goddard III, W. A. The Reaction Mechanism of the Enantioselective Tsuji Allylation: Inner-Sphere and Outer-Sphere Pathways, Internal Rearrangements, and Asymmetric C-C Bond Formation. *J. Am. Chem. Soc.* **2012**, *134*, 19050–19060.
- (92) Frisch, M. J.; Trucks, G. W.; Schlegel, H. B.; Scuseria, G. E.; Robb, M. A.; Cheeseman, J. R.; Scalmani, G.; Barone, V.; Mennucci, B.; Petersson, G. A.; Nakatsuji, H.; Caricato, M.; Li, X.; Hratchian, H. P.; Izmaylov, A. F.; Bloino, J.; Zheng, G.; Sonnenberg, J. L.; Hada, M.; Ehara, M.; Toyota, K.; Fukuda, R.; Hasegawa, J.; Ishida, M.; Nakajima, T.; Honda, Y.; Kitao, O.; Nakai, H.; Vreven, T.; Montgomery, J. A., Jr.; Peralta, J. E.; Ogliaro, F.; Bearpark, M.; Heyd, J. J.; Brothers, E.; Kudin, K. N.; Staroverov, V. N.; Kobayashi, R.; Normand, J.; Raghavachari, K.; Rendell, A.; Burant, J. C.; Iyengar, S. S.; Tomasi, J.; Cossi, M.; Rega, N.; Millam, N. J.; Klene, M.; Knox, J. E.; Cross, J. B.; Bakken, V.; Adamo, C.; Jaramillo, J.; Gomperts, R.; Stratmann, R. E.; Yazyev, O.; Austin, A. J.; Cammi, R.; Pomelli, C.; Ochterski, J. W.; Martin, R. L.; Morokuma, K.; Zakrzewski, V. G.; Voth, G. A.; Salvador, P.; Dannenberg, J. J.; Dapprich, S.; Daniels, A. D.; Farkas, Ö.; Foresman, J. B.; Ortiz, J. V.; Cioslowski, J.; Fox, D. J. Gaussian 09, Revision D.01; Gaussian, Inc.: Wallingford, CT, 2009.
- (93) Marenich, A. V.; Cramer, C. J.; Truhlar, D. G. Universal Solvation Model Based on Solute Electron Density and on a Continuum Model of the Solvent Defined by the Bulk Dielectric Constant and Atomic Surface Tensions. *J. Phys. Chem. B* **2009**, *113*, 6378–6396.
- (94) To properly account for the solvation effects on entropy, molecular dynamics simulations using explicit solvent (water) are typically required. This is beyond the scope of the current study. See: (a) Levy, R. M.; Gallicchio, E. Annu. Rev. Phys. Chem. 1998, 49, 531.
- (b) Wan, S.; Stote, R. H.; Karplus, M. J. Chem. Phys. 2004, 121, 9539. (95) Plata, R. E.; Singleton, D. A. A Case Study of the Mechanism of Alcohol-Mediated Morita-Baylis-Hillman Reactions. The Importance of Experimental Observations. J. Am. Chem. Soc. 2015, 137, 3811—
- (96) Leslie, A. K.; Li, D. D.; Koide, K. Amine-Promoted (-Elimination of a -Aryloxy Aldehyde for Fluorogenic Chemodosimeters. J. Org. Chem. 2011, 76, 6860–6865.